

See discussions, stats, and author profiles for this publication at: <https://www.researchgate.net/publication/51083356>

# Coarse-Grained Molecular Dynamics Simulation of DNA Trans location in Chemically Modified Nanopores

ARTICLE in THE JOURNAL OF PHYSICAL CHEMISTRY B · MAY 2011

Impact Factor: 3.3 · DOI: 10.1021/jp101052x · Source: PubMed

---

CITATIONS

14

---

READS

65

## 4 AUTHORS, INCLUDING:



Abhijit Ramachandran

19 PUBLICATIONS 144 CITATIONS

[SEE PROFILE](#)



Yaling Liu

Lehigh University

81 PUBLICATIONS 1,111 CITATIONS

[SEE PROFILE](#)

# Coarse-Grained Molecular Dynamics Simulation of DNA Translocation in Chemically Modified Nanopores

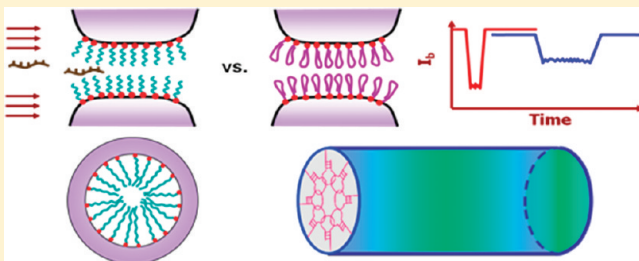
Abhijit Ramachandran,<sup>†</sup> Qingjiang Guo,<sup>‡</sup> Samir M. Iqbal,<sup>†,§,||</sup> and Yaling Liu<sup>\*,‡,⊥</sup>

<sup>†</sup>Department of Bioengineering, Joint Biomedical Engineering Program, University of Texas at Arlington and the University of Texas Southwestern Medical Center at Dallas, Arlington, Texas 76019, United States

<sup>§</sup>Nanotechnology Research and Teaching Facility and <sup>||</sup>Department of Electrical Engineering, University of Texas at Arlington, Arlington, Texas 76019, United States

<sup>‡</sup>Department of Mechanical Engineering and Mechanics and <sup>⊥</sup>Bioengineering Program, Lehigh University, Bethlehem, Pennsylvania 18015, United States

**ABSTRACT:** Solid-state nanopores provide a direct means to detect and analyze DNA and proteins. In a typical setup, the DNA molecules travel through a nanopore under electrophoretic voltage bias. The nanopore is sandwiched between two chambers that are filled with ionic solution. A major challenge in using solid-state nanopores for DNA sequencing and gene detection is to improve their selectivity and detection sensitivity. To achieve these goals, one solution is to functionalize the nanopores by chemically modifying the pore walls with silanes or nucleic acids. However, little is known about molecular interactions in functionalized nanopores. This paper presents DNA translocation dynamics and the mechanism of DNA sequencing in a functionalized nanopore through a coarse-grained molecular dynamics model. The DNA nucleotide is coarse-grained into two interaction sites: one site corresponds to the base group and the other encompasses the phosphate and sugar groups. The water molecules are included in the model implicitly through Langevin dynamics. The coarse-grained model immensely improves the computational efficiency while still capturing the essential translocation dynamics. The model characterizes important physical properties of functionalized nanopores such as the effective pore diameter and effect of biasing voltage on the DNA translocation dynamics. The model reveals a nonlinear relationship between translocation speed of DNA and applied voltage. Moreover, DNA translocation in nanopores functionalized with hairpin-loop (HPL) DNA and single-stranded DNA (ss-DNA) shows significant differences: a target DNA is found to translocate through a ss-DNA coated nanopore 9 times faster than through an HPL coated one at a bias of 100 mV, putatively from lower stiffness of ss-DNA than that for HPL. The DNA translocation speed is also largely influenced by interaction potential between the DNA and surface-tethered molecules. The results reveal that such selective translocation, distinctly different translocation dynamics of target DNA molecules largely stem from the flexibility and orientation of the surface-tethered molecules. These findings can significantly impact the rational design of DNA transport experiments leading to rapid molecule-level diagnostics.



## 1. INTRODUCTION

Microfabrication technology has made it possible to make a variety of micro- and nanofluidic devices for biochemical analysis. An area of increased development and exciting opportunities is the use of solid-state nanopores. The silicon-based pores are fabricated in suspended thin membranes at true nanometer dimensions. Such nanopores are fabricated in many ways including TEM beam-mediated drilling of a membrane,<sup>1,2</sup> adatom movement under a tightly focused electron beam, ion beam sculpting,<sup>3</sup> and thermal shrinking.<sup>4</sup> Nanopores provide high throughput for rapid manipulation, biophysical studies, and sequence identification of single DNA molecules. The basic idea of the translocation experiment relies on the movement of negatively charged DNA in an electrophoretic field. Under an applied electric field, the DNA molecule is driven through a nanopore in a linear head-to-tail fashion. This movement, called

“translocation”, is detected as an ionic current dip, also called a “pulse”, when the DNA molecule mechanically blocks a finite volume of the nanopore, thus reducing the amount of flowing ionic species through the nanopore.<sup>5,6</sup> Statistical analysis of these pulses shows trends that are direct manifestation of various physical properties of the translocating DNA molecule such as their mechanical properties,<sup>7</sup> mobility of DNA molecule in relation to its size,<sup>8</sup> and effects of factors such as salt concentration or fluid viscosity on DNA molecule translocation.<sup>1,2</sup> Theoretical studies using molecular dynamics (MD) have helped in understanding the translocation kinetics and dynamics of single- and double-stranded DNA (ss-DNA and ds-DNA) through

**Received:** February 3, 2010

**Revised:** March 23, 2011

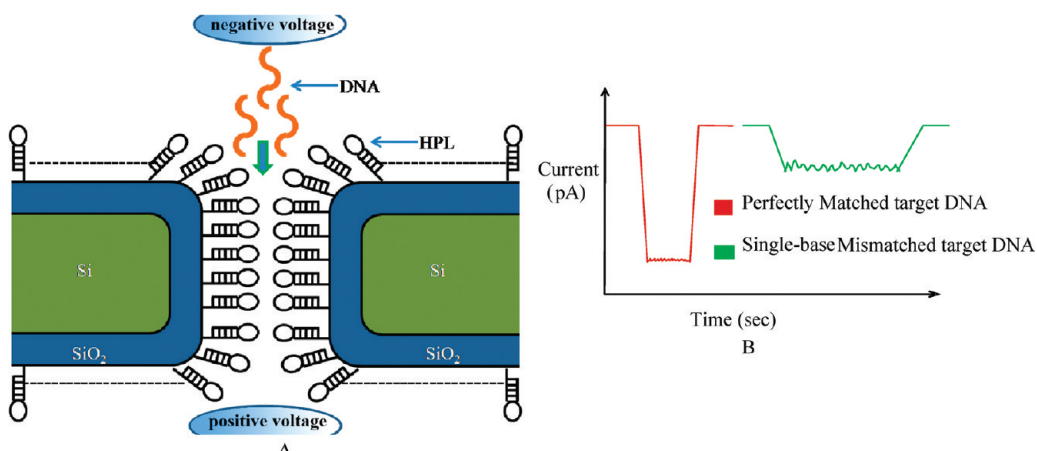


**Figure 1.** (A) Schematic of a hairpin loop DNA functionalized nanopore system (not to scale). (B) Conceptual ion current traces which show that selectivity of matched and mismatched DNA molecules is measured from the differences in translocation times (measured between the start and end of the pulses in ionic current trace) and pulse amplitude, adapted from ref 18, by permission from Macmillan Publishers Ltd: *Nat. Nanotechnol.*, copyright (2007).

nano pores,<sup>9,10</sup> to correlate the ionic current modulations to the translocating DNA sequence<sup>11</sup> and also to describe the electro-mechanical properties of translocating DNA.<sup>12</sup>

While it is easy to detect the passage of a DNA through the pore based on the modulation of the current, it is far more difficult to identify the individual bases/nucleotides. Such identification may be implemented using a strategy similar to the one present in natural systems. Cell membranes have ion channels that recognize and selectively regulate the molecule flux across the membrane. These ion channels show exquisite selectivity indicating the presence of recognition elements inside the channels. Analogously, the nanopores can be functionalized with known “recognition” molecules which have the ability to bind to target sequences. Such a scheme provides the recognition of a specific target molecule in an unknown sample based on DNA target binding with a functionalized molecule and can accordingly facilitate or hinder the transport of the target sequence. The corresponding modulation of ion current can be used to decode the DNA sequence. To achieve this, solid-state nanopores are chemically modified by silane coatings,<sup>13–16</sup> DNA,<sup>17–19</sup> or peptide–nucleic acid,<sup>20</sup> to enable molecular selectivity to detect a single base, gene, or protein of choice.<sup>21–24</sup> Such functionalization not only changes surface properties such as charges and hydrophobicity, but also results in different molecular interactions, amounts of drag, and hybridization rates. For example, Kohli et al. have demonstrated a membrane with selective permeation which recognized and transported only those DNA strands that were perfect complementary to the transporter strand attached to the inner walls of the nanotubes.<sup>19</sup> Iqbal et al. illustrated single-molecule electrophoretic transport measurements of ss-DNA through hairpin loop functionalized nanopores.<sup>18</sup> Hairpin-loop DNA (HPL) was used for molecular recognition to detect short DNA targets with single-base selectivity.

As illustrated in Figure 1A, when a target DNA passes through a nanopore under an applied bias in a head-to-tail fashion, the interaction between the target DNA and probe DNA (covalently attached to the nanopore surface) blocks the ionic current and leads to different translocation kinetics (speed and amplitude). The ionic current signature is used to determine if the sequence of a target DNA matches with that of the probe DNA. Figure 1B

conceptually illustrates typical ionic current signatures for complementary and mismatched DNA molecules translocating through a nanopore functionalized with a hairpin-loop molecule coating.<sup>18</sup>

In the long run, various applications of solid-state nanopores for DNA sequencing, protein identification, or pathogen detection will require very precise control of nanopore size, balance of applied bias voltage with molecular interactions, and test conditions. The current understanding of the DNA–nanopore interaction mechanism is still limited due to the small size of the nanopore/DNA and the dynamic translocation process inside the nanopore. Little is known about the orientation and behavior of DNA in the nanopore environment under varying biases, pore properties, and surface functional groups. Fundamental understanding of such a bionano system will ultimately lead to a new generation of integrated systems that combine the unique properties of the nanopores with biological recognition capabilities. A few attempts have been made to explore the DNA–nanopore or DNA–nanotube interaction through atomistic molecular dynamics, coarse-grained molecular dynamics (CGMD),<sup>25,26</sup> and mesoscale models.<sup>27</sup> Molecular dynamics (MD) modeling is capable of capturing essentially all phenomena in the DNA–nanopore interactions. The approach of all-atom MD simulations has undergone tremendous developments from a methodology which, six years ago, could only afford simulations of a few thousand atoms and a few nanoseconds<sup>28</sup> to one that now permits simulations of tens of millions of atoms and tens of microseconds.<sup>11</sup> However, despite this development, modeling the above-described process using the all-atom approach remains a formidable challenge. Given the length (nanometers to micrometers) of a DNA chain and the time scale (nanoseconds to seconds) involved in the general on-chip DNA diagnosis, fulfilling this work using only MD simulations is impractical.

In this paper, a coarse-grained (CG) simulation approach is presented that models the DNA translocation through a functionalized solid-state nanopore while retaining the essential dynamics at molecular scale. First, a CG model of DNA and a functionalized nanopore is described. This is followed by characterization of interactions between a translocating DNA and various chemically modified nanopores. Finally, translocation processes of a DNA with sequence perfectly matching the probe

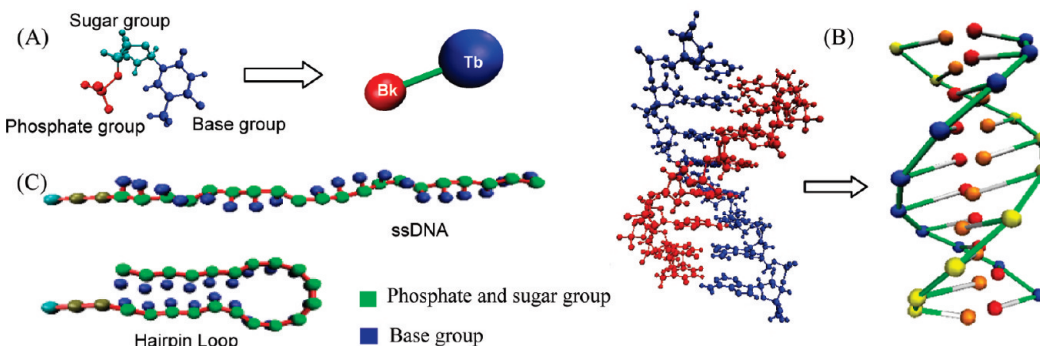


**Figure 2.** Coarse-grained DNA model. (A) Coarse graining of a thymine nucleotide into two sites. (B) Coarse graining of a double-stranded DNA. (C) Coarse-grained single-stranded DNA and hairpin-loop DNA.

molecules are compared to that with a mismatched sequence, revealing the underlying molecular mechanisms of nanopore-based DNA sequencing.

## 2. COARSE-GRAINED MODEL FOR DNA TRANSLOCATION IN A FUNCTIONALIZED NANOPORE

**2.1. Coarse-Grained DNA Model.** In recent years, various CG DNA models have been developed.<sup>29–31</sup> CG models using a two-site DNA representation have been used by Zou et al.<sup>26</sup> in characterizing DNA interactions with carbon nanotubes and by Höfler et al.<sup>25</sup> to study the electromechanical gating effect in DNA modified conical nanopores. Höfler et al.<sup>25</sup> developed a CG model based on work by Marrink et al.,<sup>35</sup> while Zou et al.<sup>26</sup> adapted the two-site DNA model from Drukker et al.<sup>33</sup> In this work, we have introduced charge on the backbone (center of mass of sugar and phosphate) of the two-site model following a similar approach by Knotts et al.,<sup>31</sup> where a three-site DNA model with negative charge on the phosphate was reported. Maffeo et al.<sup>34</sup> have described the use of negative charges and screening electrostatic potential for DNA–DNA electrostatic interactions. The model we have adopted is relatively simple but accurate enough to be extended to capture the DNA–nanopore and DNA–DNA interaction dynamics at the atomic scale. This CG model for DNA is established by first grouping atoms into a few interaction sites, followed by the construction of equivalent intersite interaction potentials. For example, a thymine nucleotide, which comprises of 32 atoms, can be coarse-grained into two interaction sites:<sup>29</sup> the backbone site (Bk, representing the sugar and phosphate groups) and the base site (Tb), as shown in Figure 2A. There are four types of base sites corresponding to four bases of DNA (adenine (A), thymine (T), cytosine (C), and guanine (G)). The coarse-graining scheme is illustrated in Figure 2.

To construct an equivalent intersite interaction potential, a preselected analytical function was parametrized by matching the thermodynamic properties from the full-atom MD simulations with those from experiments.<sup>31</sup> The total energy of the DNA molecules can be generally expressed as

$$E_{\text{total}} = E_{\text{bond}} + E_{\text{angle}} + E_{\text{dihedral}} + E_{\text{bp}} + E_{\text{stack}} + E_{\text{ex}} + E_{\text{qq}} \quad (1)$$

Parameters of the model are listed in Table 4 in the Appendix. These three terms of eq 1 describe the bonded intersite interactions including bond stretching, bending, and torsion. The last four terms are pairwise potentials which describe the nonbonded

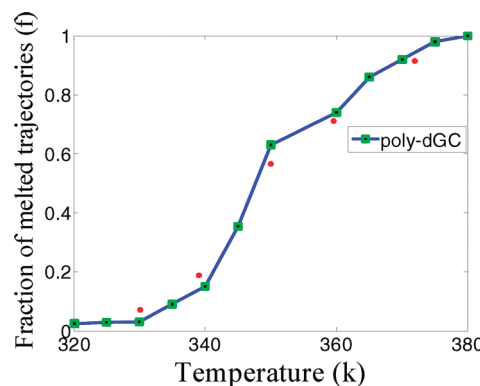


**Figure 3.** Melting curve for d(CG) DNA: fraction of trajectories ( $f$ ); DNA strands separated as a function of temperature. As the temperature gradually increases from 320 K, the DNA strands begin to separate and the fraction  $f$  increases and becomes almost 1 at 380 K, i.e., when the two strands are completely separated.

interactions. The nonbonded interactions include  $E_{\text{stack}}$ , which accounts for the base stacking phenomena,  $E_{\text{bp}}$ , which depicts hydrogen bonding between complementary base pairs,  $E_{\text{ex}}$ , which describes an excluded volume that spans energy interactions among A, T, C, and G bases, and  $E_{\text{qq}}$ , which caters for electrostatic interactions. The  $E_{\text{bp}}$  term is critical for modeling the hybridization of a ss-DNA with a complementary or hairpin loop ss-DNA.  $E_{\text{bp}}$  was parametrized using thermal denaturation experimental data at a fixed salt concentration of  $\sim 0.1$  M. At room temperature ( $\sim 300$  K), two ss-DNA strands hybridized into a stable ds-DNA; thus the fraction of separated DNA bases was close to zero.

As shown in Figure 3, the fraction of the melted DNA strands increased as the temperature increased, reaching a value of 1 when the temperature was close to 380 K.<sup>32</sup> These results are in agreement with the experimental data<sup>33</sup> marked as red circles in Figure 3, given that the DNA sequence used is the same (d(CG)).  $E_{\text{bp}}$  was described as a function of the donor–acceptor distance  $r$  and the angle  $\phi$  between the backbone, donor, and acceptor. A preassumed form was chosen for  $E_{\text{bp}}$  as<sup>33</sup>

$$E_{\text{bp}} = (E_{\text{bp}1}(r) - E_{\text{bp}2}(r))f(\phi) \quad (2)$$

with

$$f = \frac{1}{2}(\cos(\phi\gamma) + 1), \quad \phi^{\min} \leq \phi \leq \phi^{\max}$$

$$f = 0, \text{ otherwise}$$

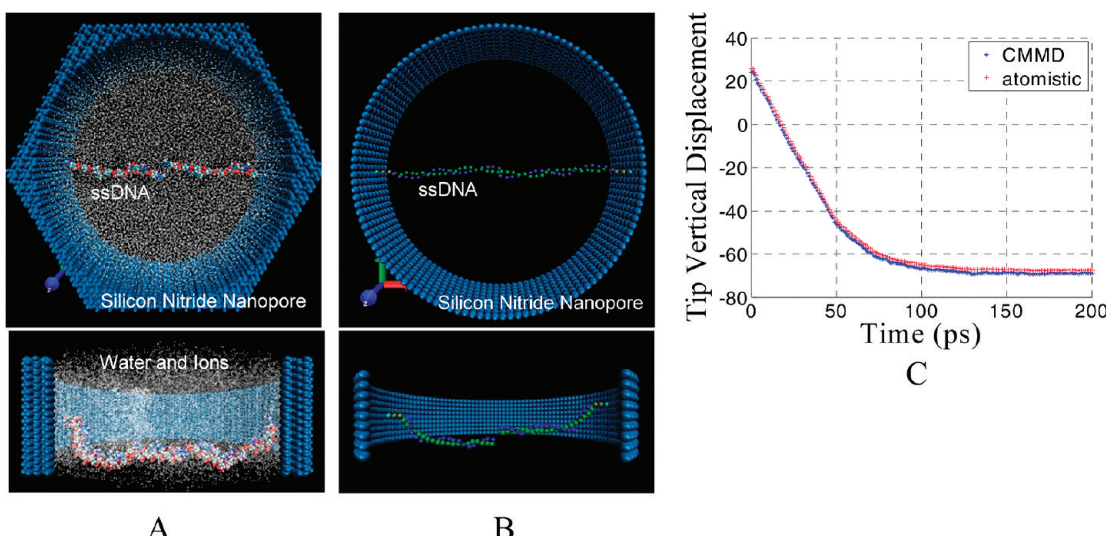


**Figure 4.** Benchmark case comparing all-atom MD (A) and CGMD (B) systems. Two ss-DNA molecules are fixed to the inner circumference of the nanopores with one end of each of these strands covalently attached to the wall. (C) The average tip displacement (angstrom) was measured as a function of time under an E-field of 0.1 V/nm.

$E_{\text{bp}1}$  describes the donor–acceptor interactions,  $E_{\text{bp}2}$  describes the solvent effect, and the  $f(\phi)$  term restricts the angle  $\phi$  in hydrogen bond to a certain range.

The DNA–DNA electrostatic interactions were described by a screened electrostatic potential:<sup>34</sup>

$$E_{\text{qq}} = \frac{q_{\text{eff}}}{\varepsilon r} \exp\left(\frac{-r}{\lambda_D}\right) \quad (3)$$

where the effective charge  $q_{\text{eff}}$  was chosen to be 40% of the nominal charge density,<sup>34</sup> given loose condensation of shielding charges in the major and minor grooves of DNA.

To ensure that the CG model accurately described the molecular motion, a benchmark case was performed by comparing the all-atom MD with the CG results. Under the application of an electric field (E-field) of 0.1 V/nm, the dynamics of two separate ss-DNAs with one end functionalized (fixed) on the inner circumference of a nanopore was studied by both all-atom MD and the CG model, as shown in Figure 4. The application of the E-field caused the ss-DNA to stretch in the direction of the field. The DNA motion was characterized by the displacement of the free end of the ss-DNAs. The average tip displacement of ss-DNA obtained from both full atomistic simulation and CG simulation were plotted as a function of time (Figure 4(C)). The CG results agreed well with the full-atomistic results. This benchmark case illustrated that our CG system can capture the essential translocation kinetics as observed in full-atomistic simulations, thus confirming the validity of the developed CG system. However, it should be noted that such a CG system does not properly describe the distribution of the electrostatic field in the nanopore.

**2.2. Coarse-Grained DNA–Nanopore Interaction Potential.** The interaction between each CG site and the nanopore surface was characterized by a Lennard-Jones (LJ) potential with parameters extracted from all-atom molecular dynamics (MD) simulations through a variational minimization and energy matching procedure,<sup>26,36–39</sup> which are listed in Table 1. The setup of the all-atom MD simulation was the same as that described by Ramachandran et al.<sup>9</sup> All-atom MD simulations

**Table 1. LJ Interaction Potential Parameters between the Nanopore and Each CG DNA Site Extracted from All-Atom MD Simulations**

interaction sites	backbone	base			
		ADE	GUA	CYT	THY
$\sigma$ (nm)	0.492	0.404	0.411	0.383	0.392
$\varepsilon$ (kJ mol <sup>-1</sup> )	3.860	5.913	6.195	5.687	5.846

were performed in NAMD<sup>40</sup> (NAnoscale Molecular Dynamics), while CG simulations were done in GROMACS.<sup>41</sup> The CHARMM<sup>42</sup> force field was used for the DNA in the all-atom model. For the silicon nitride ( $\text{Si}_3\text{N}_4$ ) pore, the force field describing  $\text{Si}_3\text{N}_4$  was transcribed in terms of the potential functions used in the CHARMM force field.<sup>28</sup> The water molecules were described by TIP3P potential in the all-atom model. The total potential energy was composed of bonded energies and nonbonded pair interaction energies.<sup>43</sup>

The LJ potential parameters chosen for the CG model accurately reproduced the trajectory and energy data from all-atom MD simulations. The CG DNA–surface potential was combined with the CG DNA model explained in section 2.1 to model the full dynamic process of a ss-DNA translocation in a nanopore. For a functionalized nanopore, the CG DNA model readily handled interactions between surface-tethered probe (ss-DNA or HPL DNA) and translocating DNA through the base pair interactions described in section 2.1.

**2.3. Coarse-Grained Simulations of DNA Translocation in Surface-Modified Nanopore.** The established CG DNA model and the DNA–nanopore interaction potential enabled the CG simulation of DNA translocation in a surface modified nanopore. To further reduce the computational time, the solvent effect was included implicitly as stochastic frictional forces through Langevin dynamics. It should be noted that the introduction of the implicit solvent eliminated the electrokinetic effects that would have stemmed from the electroosmotic flow,<sup>44</sup> while it did not significantly affect the surface interaction based DNA

translocation kinetics. In Langevin dynamics, the friction constant  $\xi$  is related to solvent viscosity  $\eta$  by  $\xi = 4\pi\eta r_{\text{eff}}/m$ , where  $r_{\text{eff}}$  is the solute's effective hydrodynamic radius and  $m$  is the mass of CG particles.

In addition to a substantially reduced number of the degrees of freedom, the CG model allowed the use of a significantly larger time step ( $\sim 10$  fs) compared to that possible with molecular dynamics ( $\sim 1$  fs) in the simulations since the high-frequency modes of individual atoms could be suppressed. Thus, this model substantially improved computational affordability while preserving details of the molecular kinetic features. Considering the real experimental conditions where a large number of molecules are functionalized on the nanopore surface and the translocation time is a few microseconds for short DNA molecules, such a CG DNA model was necessary for exploring the full translocation process of a DNA in a nanopore with various surface coatings.

In the simulations, the temperature was set at 300 K and a time step of 0.01 ps was used. Nonbonded interactions were cut off at 1.2 nm, and the Lennard-Jones potential was smoothly shifted to zero in the region starting from 1 nm from the pore wall surface up to the cutoff distance. The pair list was updated every step using a 1.4 nm cutoff distance. Periodic boundary conditions were applied at the entrance and outlet of the pore. Visualization and analysis were done with Visual Molecular Dynamics (VMD)<sup>45</sup> and MATLAB scripts. All simulations were performed on the supercomputer cluster Ranger at Texas Advanced Computing Center (TACC), which is part of the Teragrid resources.<sup>46</sup> A 200 ns simulation on two processors took around 24 h. The number of atoms in the system varied with the size of the configuration considered. A typical CG system had 4714 atoms with 2610 atoms for the Si<sub>3</sub>N<sub>4</sub> pore, 1960 atoms for DNA functionalized on the surface, and 40 atoms accounting for the translocating DNA. To simulate translocation events within the MD time limit, the CGMD simulations were performed in applied bias voltages ranging between 50 and 500 mV.

### 3. RESULTS

The biofunctionalization approach introduces molecular selectivity to the nanopores. The selectivity of a functionalized nanopore largely depends on the chemical groups available on the intermediate coatings (e.g., silanes) and the properties of surface-tethered molecules such as stiffness, contour, arrangement, and charge, all under an applied bias voltage. These factors impact the effective pore diameter and translocation kinetics which ultimately results in different behaviors for different target molecules. The translocation process thus needs careful characterization of the parameters involved. In recent years, a number of research efforts have shown the use of a variety of molecular coatings on nanopores, which interact with the translocating DNA (t-DNA) in different ways. This work focuses on two types of probe molecules used to functionalize nanopores: ss-DNA and HPL DNA (Figure 2C). Under an applied E-field, the surface-bound molecules reorient along the E-field due to their inherent negative charges. The magnitude of bending depends on a molecule's rigidity, shape, structure, and intrastrand bonds. A measurement of the behavior of the molecular structures and morphology is the effective pore diameter (EPD), which is the diameter of the empty space in the center not occupied by loose ends of the surface-bound molecules, as illustrated in Figure 5. The characterization of the EPD of a biofunctionalized nanopore system depends on three groups of parameters: type of surface

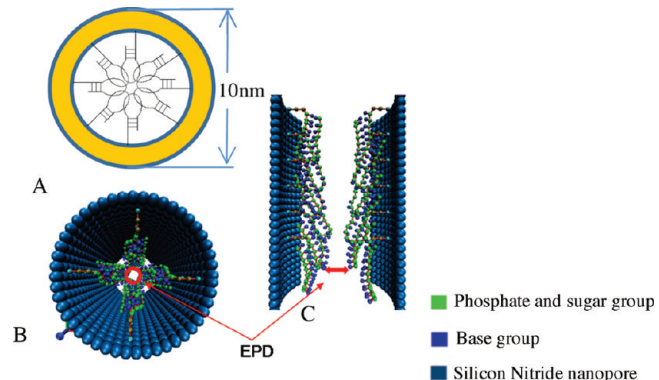


**Figure 5.** Effective pore diameter (EPD): diameter of the empty space in the center of the biofunctionalized nanopore not occupied by surface-bound molecules.

functionalization, density of molecular self-assembled monolayer (SAM), and applied bias voltage. The results of the effects of these parameters are summarized and presented in the Appendix.

**3.1. Influence of Interaction Potential on Translocation Dynamics.** The velocity of the translocating DNA largely depends on its interaction with the surface-bound probe molecules. In particular, probe DNA molecules of different sequences have different binding energies. For example, a C·G pair has a higher binding energy than an A·T pair.<sup>28</sup> Such differences in binding energies can be used to extrapolate sequence information of the translocating DNA. In this section, the focus is to characterize the influence of interaction between probe DNA and t-DNA on the translocation of t-DNA. Two typical cases were considered: t-DNA with all complementary bases (such as CCCCCGGGGTTTTGGGGG) and t-DNA with completely mismatched bases (such as AAAAAAAAAAAAAA-AAAAAAAA) with respect to the probe DNA (such as GGGGGCCCCCAAAAACCCCC). Since the complementary t-DNA usually has attractive interaction with probe DNA while the mismatched DNA has neutral (or weak) interaction with probe DNA, we generally call these two cases the attractive potential case and the neutral potential case, respectively.

Due to the confinement of nanopore on both probe DNA and t-DNA, the model system was built in four steps. The initial step was to place a single DNA strand with one end covalently attached to the nanopore surface in the given E-field for 100 ns. Following this, additional strands (replicates of the covalently attached single strand) were introduced into the system to maintain the desired EPD. Once the surface functionalization was complete, the system was equilibrated for 100 ns and then the t-DNA was introduced into the system. Lastly, the whole system was equilibrated for 100 ns before simulation runs. Three different probe molecule configurations were considered: HPL DNA, ss-DNA with strands placed longitudinally 1 nm apart, and ss-DNA with strands placed longitudinally 2 nm apart. The circumferential densities of the strands were constant for all three coating systems.

The modeled systems covered EPD ranging from 1 to 8 nm (Figure 6), sufficient to understand the weak and strong interactions between the probes and the t-DNA. Nanopores were functionalized with DNA strands of 20 bases with sequence GGGGGCCCCCAAAAACCCCC, t-DNA was 20 bases long with the sequence CCCCCGGGGTTTTGGGGG for attractive potential cases, and t-DNA for the neutral potential cases

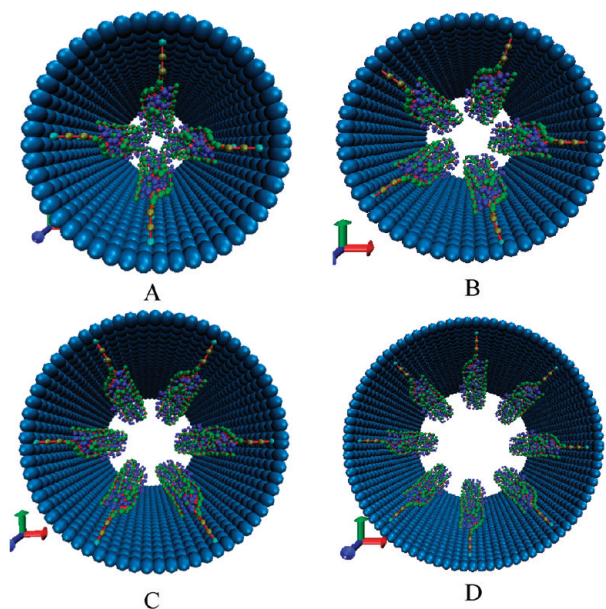


**Figure 6.** Illustration of different effective pore diameter cases studied: (A) 1, (B) 2.8, (C) 4.6, and (D) 8.1 nm.

**Table 2. Summary of Sequences of DNA of 20 Bases Used As Coatings and t-DNAs for Different Cases**

(A) Sequences Used To Study the Effect of Probe DNA and t-DNA Interaction	
sequence of probe DNA functionalized on the nanopore walls	GGGGGGCCCCCAAAACCCCC
sequence of perfect complementary t-DNA (attractive potential case)	CCCCCGGGGGTTTTGGGGG
sequence of mismatched t-DNA (neutral potential case)	AAAAAAAAAAAAAAAAAAAAAA
(B) Sequences Used in Figure 10 To Study the Influence of Probe Type	
HPL DNA with closed loop functionalized nanopore	HPL: GGGGGCCCCCAAAACCCCC t-DNA: AAAAAAAAAAAAAAAAAAAA
opened HPL case (ss-DNA)	ss-DNA: GGGGGCCCCCAAAACCCCC t-DNA: CCCCCGGGGTTTTGGGGG

had the sequence of AAAAAAAAAAAAAAAAAAAA. The DNA sequences used are summarized in Table 2. To understand the influence of each parameter on t-DNA velocity, two sets of simulations were performed. The first set increased EPD, thus reducing interactions between the probe DNA and t-DNA of matched (attractive) and mismatched (neutral) cases. The second set varied the E-field from 0.01 to 0.5 V/nm at a constant EPD of 2.8 nm, thus gradually making the E-field a dominant force. The simulation results (Figures 7 and Figure 8) include both the mean and standard deviation based on five independent runs.

The results from the first set of runs of varying EPDs at a constant E-field of 0.1 V/nm indicated that the DNA

translocation velocity under a neutral potential was significantly higher than that with an attractive potential at EPD less than 3 nm, as shown in Figure 7. For example, a t-DNA traveled twice as fast in a nanopore of 1 nm EPD, functionalized with HPL with neutral potential compared to that with an attractive potential. This is mainly due to the large interaction between the t-DNA and the surface-bound probes at 1 nm EPD. As the EPD increased, the interaction between the t-DNA and the probes weakened; thus the influence of interaction potential reduced. It is interesting to note here that the t-DNA translocation velocity with EPD above 3 nm was slightly lower in a nanopore with neutral potential in comparison to that with attractive potential. Such a transition in t-DNA translocation velocity from attraction unfavorable to attraction favorable happened at EPD around 3–4 nm. These results suggest that weak attractive potential enhanced t-DNA translocation, while strong attractive potential hindered the t-DNA translocation; further studies are thus under way to confirm this observation. The interstrand potential was one of the major factors in determining the kinetics of t-DNA translocation.

To explore further the influence of interaction potential on translocation dynamics, a nanopore with a fixed EPD of 2.8 nm was used to calculate the velocity of t-DNA at different voltage biases applied across the nanopore. As shown in Figure 8, the translocation velocities in a nanopore with neutral potential are higher than those with attractive potential. This can be explained by the fact that stronger interaction forces hold t-DNA locally and slow down the passage. As the bias voltage increased, the difference in velocities reduced since the E-field was dominant over interstrand interaction potential. The significant differences in t-DNA velocity under different potentials at lower E-fields suggest that the DNA translocation process can be modulated by the strength of its interaction with the surface-bound probe molecules.

**3.2. Influence of Coating Type on Translocation Dynamics: Mechanism of Selectivity.** Selectivity is the key feature of a functionalized nanopore, yet little is known about the exact mechanism of selectivity due to the small size of the nanopore and the complex dynamic process. In previous sections, the various parameters have been analyzed that influence DNA translocation, including type of probe DNA, density of probe DNA, interaction potential, EPD size, and E-field. In this section, the full process of DNA translocation is mimicked in an HPL functionalized nanopore.

Recent experimental work<sup>18</sup> has demonstrated that a nanopore functionalized with HPL can achieve single base selectivity (Figure 1). The perfectly complementary (PC) and mismatched (MM) t-DNAs were transported through HPL–nanopore under an electrophoresis bias. The PC ss-DNA hybridized with matching hairpin-loop DNA sequentially, which facilitated the translocation process.<sup>18</sup> Under optimal conditions in solution, the HPL DNA showed an all-or-none selectivity down to single-base mismatch sensitivity between PC and MM ss-DNA targets.

The DNA–HPL hybridization kinetics is a complex process which involves random fluctuations of HPL DNA, opening of HPL in a confined environment, hybridization of opened-HPL with t-DNA, and movement of t-DNA after sequential hybridization between adjacent probe molecules. As an initial attempt, a comparison was done between MM t-DNA translocation through a nanopore functionalized with HPL DNA and PC t-DNA translocation thorough a pore functionalized with ss-DNA from opening of HPL DNA. Figure 9 shows the translocation of

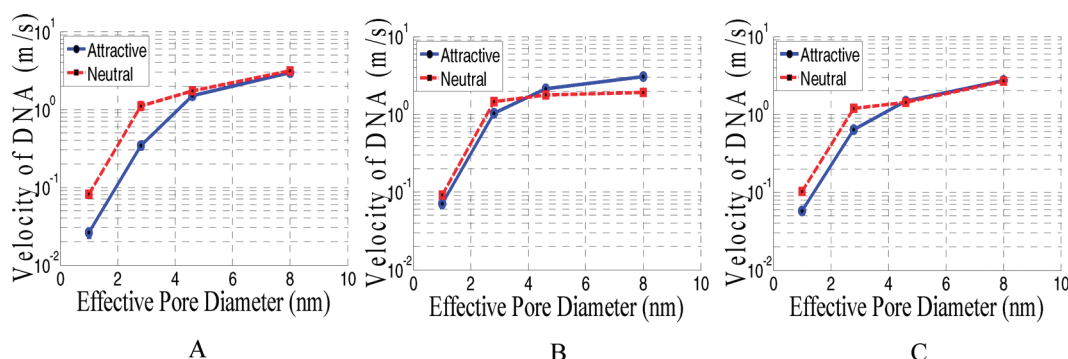


**Figure 7.** Influence of interaction potential on t-DNA translocation velocity under an E-field of 0.1 V/nm. Each plot compares the velocities of the translocating DNA (t-DNA) in a DNA functionalized nanopore of attractive and neutral potentials at different EPDs. Different probe DNA molecules considered are (A) HPL, (B) ss-DNA 1 nm apart, and (C) ss-DNA 2 nm apart.

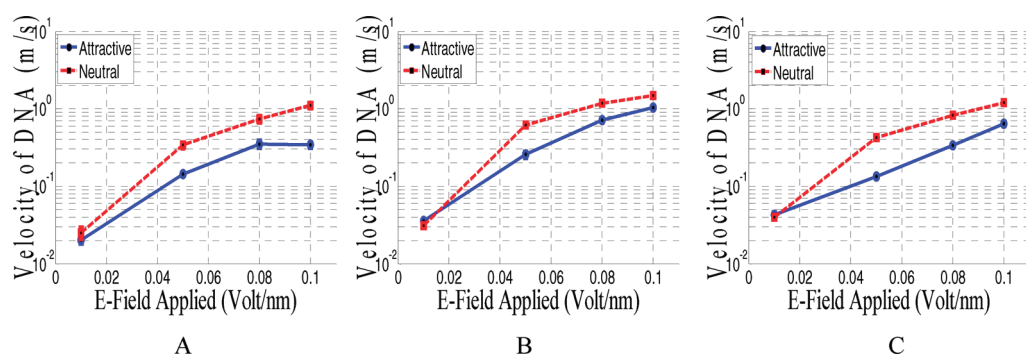


**Figure 8.** Influence of interaction potential on DNA translocation velocity at an EPD of 2.8 nm under an E-field ranging from 0.01 to 0.1 V/nm. The case for 0.5 V/nm is not shown for clarity and is given in the Appendix. Each plot compares the velocities of the translocating DNA (t-DNA) in a DNA functionalized nanopore of attractive and neutral potentials at different E-fields. The probe DNAs considered are (A) HPL, (B) ss-DNA 1 nm apart, and (C) ss-DNA 2 nm apart.

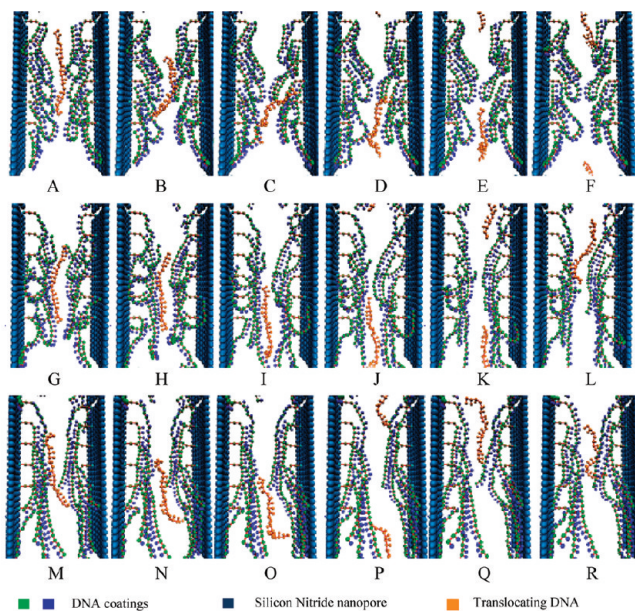


**Figure 9.** Translocation of t-DNA through (A–F) HPL functionalized nanopore, (G–L) HPL functionalized nanopore in which HPL opens up into ss-DNA, and (M–R) ss-DNA functionalized nanopore.

t-DNA in nanopores with various probes. Figure 9A–F shows the process of a MM t-DNA translocating through a HPL probe

nano pore. Figure 9G–L illustrates the process of a PC t-DNA hybridization and consequent opening of functionalized HPL when a PC molecule passes through a nanopore. Figure 9M–R demonstrates the process of a PC t-DNA translocating through a ss-DNA functionalized nanopore (this could also represent a case ignoring the HPL opening process). The surface-bound probe and translocating DNA both consist of 20 bases. DNA sequence GGGGGCCCCCAAAAACCCCC was used as a probe, while the translocating DNA was CCCCCGGGGTTTTGGGGG and AAAAAAAAAAAAAAA for the PC and MM cases, respectively (Table 2).

There were significant differences in translocation velocities of the MM and PC DNAs (Figure 10). This is because the functionalized HPLs opened up into flexible ss-DNA when they interacted with PC DNA, resulting in increased EPD under applied E-field, thus facilitating the translocation process compared that with the MM DNA. Consequently, a PC DNA had reduced translocation time, consistent with the experimental observations<sup>18</sup> where PC DNA was observed to translocate eight times faster than MM DNA at an applied voltage of 100 mV. The different translocation velocities at various applied E-field strengths are listed in Table 3.

As shown in Figure 10, a t-DNA passes through ss-DNA functionalized nanopore around nine times faster than that through HPL functionalized nanopore under an applied E-field of 10 mV/nm. Such a difference in translocation time decreased with E-field strength. This is because high E-field leads to forced translocation of DNA regardless of probe type. The results of

**Table 3. DNA Translocation Velocities in HPL and ss-DNA Coated Nanopores**

E-field (V/nm)	DNA velocity in HPL functionalized pore (m/s)	DNA velocity in ss-DNA functionalized pore (m/s)	relative increase (%)
0.01	0.001	0.01	900
0.03	0.008	0.06	650
0.05	0.04	0.1	150
0.08	0.135	0.3	122
0.1	0.48	0.88	83
0.3	3.48	4.33	24.4

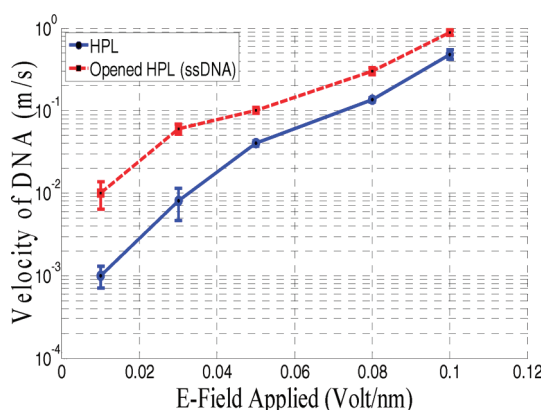


**Figure 10.** Effect of biofunctionalization on DNA translocation velocity. t-DNA translocates at different velocities in nanopores functionalized with HPL and the opened HPL (ss-DNA).

Figure 10 partially explains the selective transport mechanism of functionalized nanopores: a PC t-DNA can hybridize with the probe-HPL, opening the rigid HPL into flexible ss-DNA, thus facilitating faster translocation. In contrast, a MM DNA has to force its way through the HPL coating which is comparatively more rigid and, thus, has a longer translocation time. Figure 10 actually shows the ideal difference in translocation velocities of a MM DNA and a PC DNA, by assuming a zero hybridization time (the HPL opening process is ignored and treated directly as a ss-DNA). The concept of using biofunctionalized nanopores for DNA sequencing is a new field with very limited experimental work reported. For example, Kohli et al.<sup>19</sup> and Iqbal et al.<sup>18</sup> have studied DNA translocation in cone-shaped nanopores. The nonlinear increase of DNA translocation speed as a function of applied bias voltage agrees qualitatively with the experimental trends observed by Iqbal et al.<sup>18</sup> However, a direct quantitative comparison cannot be made between the simulation and the far more complex experimental setups. As an example, when a small bias voltage of 100–200 mV was usually applied on a nanopore over 100 nm in length with unknown surface probe density and distribution, a mean translocation time of 10 ms was measured for a perfectly matched DNA with large variations from 1 to 500 ms (standard deviation ~30 ms). These variations might be due to a range of configurations at which t-DNA could enter the pore. To capture these subtle yet significant variations, the simulations would have to be run with applied bias voltages either equal to or lower than the experimental bias voltages. This remains a challenge, and other MD simulation studies of DNA

translocation<sup>10,28</sup> as well as this one used E-fields of larger strengths compared to the experimental values to accelerate the simulation process. In addition, it was assumed that the DNA entered the pore in a head-to-tail fashion, which is the most likely configuration. In spite of these shortcomings our CGMD system does capture the nonlinear trend as observed in similar experimental studies.<sup>18</sup> These results support the hypothesis that the opening up of the HPL structures plays a significant role in facilitating the transport of the PC DNA.

#### 4. CONCLUSIONS

In conclusion, the translocation dynamics of DNA in a functionalized nanopore is studied for the first time through a coarse-grained molecular dynamics model. The translocation process is found to be influenced by the surface probe density and type, interaction potential, and applied bias voltages. To our knowledge, there are no other simulation methods that can produce the results presented in this paper.

Effective pore diameters for three types of functionalizations including ss-DNA and HPL (closed loop and open loop) are determined for a range of applied voltages. It is found that DNA translocates faster in a ss-DNA functionalized nanopore compared to a HPL functionalized nanopores, under the same applied bias voltage. This is mainly due to the difference in stiffness of the coating molecules which influences the EPD. In this case, a higher EPD is observed for a ss-DNA functionalized nanopore compared to an HPL functionalized nanopore. Moreover, with increase in voltage, less difference in translocation velocity is found, mainly due to the reduced influence of interaction between the t-DNA and the probe DNA. It was also interesting to find that the type of interaction between the t-DNA and the probe DNA significantly influenced the t-DNA translocation. While the focus of this paper was ss-DNA translocation through ss-DNA or HPL functionalized nanopore, the CG method developed is applicable to general molecular detection through functionalized nanopores. Such knowledge can be used to optimize the design of functionalized nanopores for desired molecular detection, and might eventually help shorten biosensor design cycles.

In the future, a more comprehensive model will be developed to study DNA translocation in other types of functionalized pores with different shapes and interaction energies of the molecules. Comprehensive understanding of such a bionano system could help achieve the ultimate goal of high-throughput genome sequencing.

**Supporting Information.** All the movies in the list can be downloaded from the following Web site: <http://www.lehigh.edu/~yal310/mdMovies.html>.

1. DNA translocation through HPL coated nanopore under an E-field of 100 mV with attractive potential (HPL\_100 mV\_attractive.mpg)
2. DNA translocation through HPL coated nanopore under an E-field of 100 mV with neutral potential (HPL\_100 mV\_neutral.mpg)
3. DNA translocation through ss-DNA coated nanopore under an E-field of 100 mV with attractive potential (ssDNA\_100 mV\_attractive.mpg)
4. DNA translocation through ss-DNA coated nanopore under an E-field of 100 mV with neutral potential (ssDNA\_100 mV\_neutral.mpg)

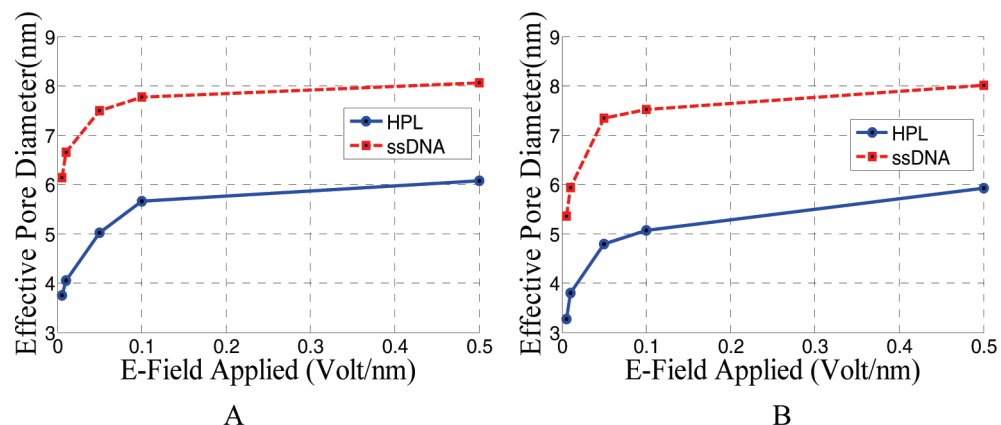


**Figure 11.** Effective pore diameter (EPD) under various E-fields for HPL and ss-DNA nanopores: (A) EPD for four-strand coating; (B) EPD for eight-strand coating.

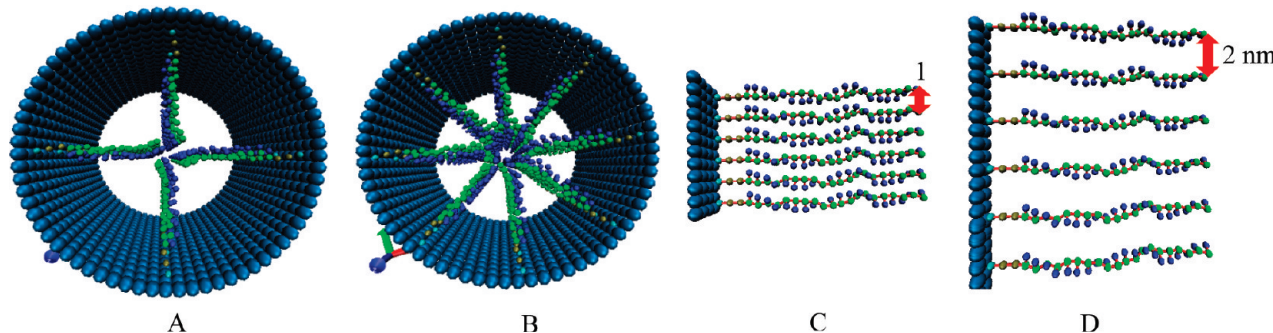


**Figure 12.** Nanopore functionalized with different circumferential and longitudinal probe DNA densities. (A) Four-strand circumferential functionalization; (B) eight-strand circumferential functionalization; (C) strands placed 1 nm apart in longitudinal direction; (D) strands placed 2 nm apart in longitudinal direction.

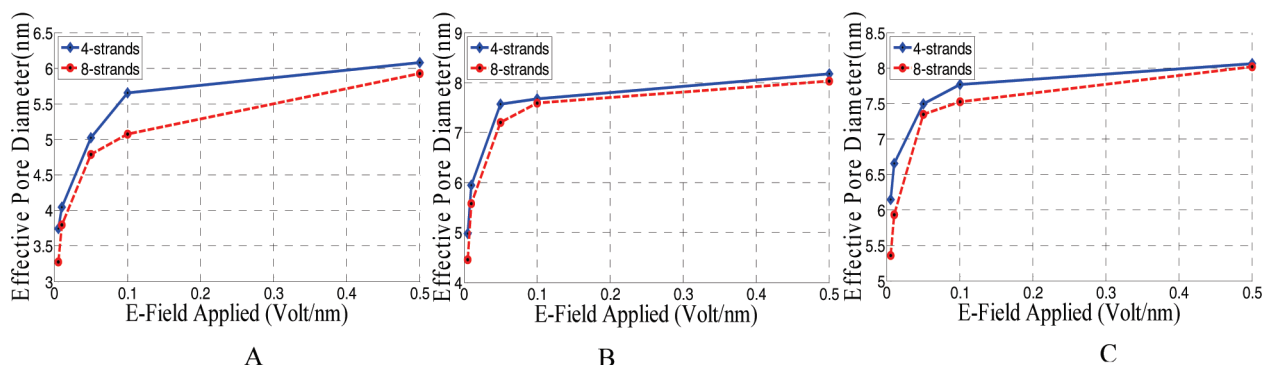


**Figure 13.** Effective pore diameter (EPD) as a function of E-field for different circumferential densities. Each graph gives a comparative analysis of the EPD obtained with the four strands functionalized to that with eight strand functionalized nanopores. Different functionalizations considered are (A) HPL, (B) ss-DNA 1 nm apart, and (C) ss-DNA 2 nm apart.

## APPENDIX

The type of functionalized probe molecules (ss-DNA or HPL) influences the effective pore diameter (EPD), which in turn influences their interaction with the t-DNA. The comparison of ss-DNA translocation through HPL functionalized nanopore with the translocation of ss-DNA through ss-DNA functionalized nanopore with a pore diameter of 10 nm gives an understanding of the effects of probe molecule type on translocation dynamics.

Both HPL and ss-DNA are widely used in molecular detection. For example, DNA microarrays use probe ss-DNA functionalized on a chip surface and its hybridization with target ss-DNA immersed in solution achieves sequence detection. HPL has also been used in DNA sequencing devices.<sup>18</sup> When a ss-DNA, with a sequence that perfectly matches with an HPL probe, translocates through the nanopore, the HPL opens up into a complementary ss-DNA, and forms a duplex. A set of simulations were performed

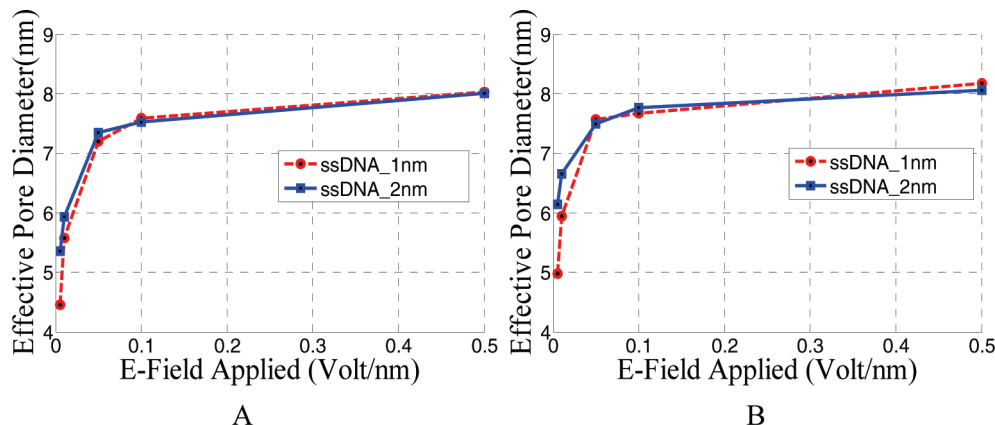


**Figure 14.** Effective pore diameter (EPD) as a function of E-field under two longitudinal densities. Different functionalizations considered are (A) four-strand circumferential functionalization and (B) eight-strand circumferential functionalization.

to understand the behavior of functionalized molecules (20 bases, GGGGGCCCCCAAAAACCCCC) under an E-field based on their molecule type, circumferential densities, and longitudinal densities.

**A.1. Influence of Coating Type on Effective Pore Diameter.** EPDs of nanopores functionalized with HPL and ss-DNA under different E-fields are shown in Figure 11. The probe molecules were assumed to be uniformly covalently attached to the nanopore surface on the pore surface. Under an applied bias voltage, the functionalized DNA reorient themselves along the E-field direction since they are negatively charged. It is clearly shown that HPL coating led to a much smaller EPD (around two-thirds) compared to that for a ss-DNA under the same applied E-field. This is because a HPL is a semistable DNA state with intrastrand hydrogen bonds that lead to a relatively rigid loop structure. In comparison with HPL, ss-DNA is highly flexible. Figure 11 indicates that a t-DNA translocating through an HPL functionalized nanopore will have more interactions in comparison with the ss-DNA functionalized nanopore. Consequently, t-DNA is expected to pass through ss-DNA functionalized pores faster than HPL functionalized pores, which is confirmed in results presented in later sections.

**A.2. Influence of Surface-Bound Probe Density on Effective Pore Diameter.** The probe density can be considered from two points of view: density in circumferential direction and density in longitudinal direction, as illustrated in Figure 12. A denser probe functionalization usually has better interaction with t-DNA. To understand the effect of probe density on translocation dynamics, the EPD and translocation properties for DNA translocation in nanopores of different probe densities can be analyzed. First, a circumferential density with four strands is compared to that of eight DNA strands, as shown in parts A and B of Figure 12, respectively. The corresponding densities of these two systems are 0.2 and 0.4 strand/nm for the four-strand and eight-strand pores, respectively.

The results shown in Figure 13 indicate a slightly smaller EPD for a nanopore with higher circumferential probe density. The EPD for nanopores functionalized with eight strands is around 15% smaller than that for pores functionalized with four strands. All three graphs show a parabolic increase of EPD with increase in applied E-field. The effect of circumferential density is more evident at lower bias voltages, especially in the less longitudinally

**Table 4. CG DNA Parameter List**

$E_{\text{bond}}$		
bonds		
	length (nm)	force constant ( $\text{kJ mol}^{-1} \text{ nm}^{-2}$ )
C—C, C—P, P—P, P—Q <sub>a</sub> (DNA)	0.435 37	41 840
Q <sub>a</sub> —N0	0.305	41 840
Q <sub>a</sub> —Q <sub>a</sub> (neighbor)	0.435 37	41 840
Q <sub>a</sub> —Q <sub>a</sub> (one Q <sub>a</sub> atom in between)	0.854 37	20 920
N0—N0 (for forming HPL)	0.47	41 840
Q <sub>a</sub> —N1	0.305	41 840
P—P (nanopore)	0.47	1 250
$E_{\text{angle}}$		
angles		
	angle (deg)	force constant ( $\text{kJ mol}^{-1}$ )
C—P—P, P—P—Q <sub>a</sub> , P—Q <sub>a</sub> —Q <sub>a</sub> , Q <sub>a</sub> —Q <sub>a</sub> —Q <sub>a</sub> (HPL)	180	334.72
N0—Q <sub>a</sub> —Q <sub>a</sub> (HPL)	90	334.72
Q <sub>a</sub> —Q <sub>a</sub> —Q <sub>a</sub> (t-DNA, ss-DNA)	157.743	334.72
Q <sub>a</sub> —N1—Q <sub>a</sub> (t-DNA, ss-DNA)	78.871	334.72
$E_{\text{dihedral}}$		
dihedrals		
	angle (deg)	force constant ( $\text{kJ mol}^{-1} \text{ rad}^{-2}$ )
HPL	180	334.72
t-DNA, ss-DNA	208.476	334.72

dense system. A large difference in the EPDs is observed between nanopores functionalized with HPL and ss-DNA.

Similarly, the longitudinal probe density also influences EPD. The comparison of two ss-DNA functionalization cases, one with the probe molecules 1 nm apart and the other with probes 2 nm apart, respectively, are shown in parts C and D of Figure 12. The importance of longitudinal density is that the interstrand

interactions between neighboring probe layers increased with increased longitudinal density. The longitudinal densities of the two systems considered are 0.12 and 0.06 strand/nm for ss-DNA placed 1 nm apart and 2 nm apart longitudinally in the pores, respectively. The results shown in Figure 14 indicate that, at low E-fields, there is a significant difference in EPD of the two systems with different longitudinal densities. The EPD for a nanopore functionalized with ss-DNA 2 nm apart is 20% higher than that for 1 nm part at the lowest E-field considered. Such difference in EPD vanishes as the applied bias voltage increases.

Table 4 gives the CG DNA parameter list for the energies in eq 1.

## AUTHOR INFORMATION

### Corresponding Author

\*Telephone: (610) 758-5839. Fax: (610) 758-6224. E-mail: yal310@lehigh.edu.

## ACKNOWLEDGMENT

Y.L. acknowledges the support of this work from the Lehigh Faculty Research Grant program, National Institutes of Health Grant EB009786-01, and National Science Foundation CBET-0955214 and TeraGrid resources. S.M.I. acknowledges support from National Institutes of Health Grant 1R43CA135960-01A1.

## REFERENCES

- (1) Smeets, R. M. M.; Keyser, U. F.; Krapf, D.; Wu, M. Y.; Dekker, N. H.; Dekker, C. *Nano Lett.* **2006**, *6*, 89.
- (2) Ho, C.; Qiao, R.; Heng, J. B.; Chatterjee, A.; Timp, R. J.; Aluru, N. R.; Timp, G. *Proc. Natl. Acad. Sci. U.S.A.* **2005**, *102*, 10445.
- (3) Li, J.; Stein, D.; McMullan, C.; Branton, D.; Aziz, M. J.; Golovchenko, J. A. *Nature* **2001**, *412*, 166.
- (4) Chang, H. *Nano Lett.* **2004**, *4*, 1551.
- (5) Kasianowicz, J. J.; Brandin, E.; Branton, D.; Deamer, D. W. *Proc. Natl. Acad. Sci. U.S.A.* **1996**, *93*, 13770.
- (6) Healy, K. *Nanomedicine (London, U.K.)* **2007**, *2*, 459.
- (7) Heng, J. B.; Aksimentiev, A.; Ho, C.; Marks, P.; Grinkova, Y. V.; Sligar, S.; Schulten, K.; Timp, G. *Nano Lett.* **2005**, *5*, 1883.
- (8) Cross, J. D.; Strychalski, E. A.; Craighead, H. G. *J. Appl. Phys.* **2007**, *102*, 024701.
- (9) Ramachandran, A.; Liu, Y.; Asghar, W.; Iqbal, S. M. *Am. J. Biomed. Sci.* **2009**, *1*, 344.
- (10) Forrey, C.; Muthukumar, M. *J. Chem. Phys.* **2007**, *127*, 015102.
- (11) Aksimentiev, A. *Nanoscale* **2010**, *2*, 468.
- (12) Heng, J. B.; Aksimentiev, A.; Ho, C.; Marks, P.; Grinkova, Y. V.; Sligar, S.; Schulten, K.; Timp, G. *Biophys. J.* **2006**, *90*, 1098.
- (13) Wang, X.; Smirnov, S. *ACS Nano* **2009**, *3*, 1004.
- (14) Danelon, C.; Santschi, C.; Brugger, J.; Vogel, H. *Langmuir* **2006**, *22*, 10711.
- (15) Wanunu, M.; Meller, A. *Nano Lett.* **2007**, *7*, 1580.
- (16) Siwy, Z.; Trofin, L.; Kohli, P.; Baker, L. A.; Trautmann, C.; Martin, C. R. *J. Am. Chem. Soc.* **2005**, *127*, 5000.
- (17) Vlassiouk, I.; Takmakov, P.; Smirnov, S. *Langmuir* **2005**, *21*, 4776.
- (18) Iqbal, S. M.; Akin, D.; Bashir, R. *Nat. Nanotechnol.* **2007**, *2*, 243.
- (19) Kohli, P.; Harrell, C. C.; Cao, Z. H.; Gasparac, R.; Tan, W. H.; Martin, C. R. *Science* **2004**, *305*, 984.
- (20) Jagerszki, G.; Gyurcsanyi, R. E.; Höfler, L.; Pretsch, E. *Nano Lett.* **2007**, *7*, 1609.
- (21) Uram, J. D.; Ke, K.; Hunt, A. J.; Mayer, M. *Angew. Chem., Int. Ed.* **2006**, *45*, 2281.
- (22) Wang, J.; Martin, C. R. *Nanomedicine (London, U.K.)* **2008**, *3*, 13.
- (23) Ali, M.; Schiedt, B.; Healy, K.; Neumann, R.; Ensinger, W. *Nanotechnology* **2008**, *19*, 85713.
- (24) Gyurcsányi, R. E. *TrAC, Trends Anal. Chem.* **2008**, *27*, 627.
- (25) Höfler, L.; Gyurcsányi, R. E. *Electroanalysis* **2008**, *20*, 301.
- (26) Zou, J.; Liang, W.; Zhang, S. *Int. J. Numer. Methods Eng.* **2010**, *83*, 968.
- (27) Liu, Y.; Iqbal, S. M. *Appl. Phys. Lett.* **2009**, *95*, 223701.
- (28) Aksimentiev, A.; Heng, J. B.; Timp, G.; Schulten, K. *Biophys. J.* **2004**, *87*, 2086.
- (29) Drukker, K.; Wu, G. S.; Schatz, G. C. *J. Chem. Phys.* **2001**, *114*, 579.
- (30) Mielke, S. P.; Gronbech-Jensen, N.; Krishnan, V. V.; Fink, W. H.; Benham, C. *J. Chem. Phys.* **2005**, *123*, 124911.
- (31) Knotts, T. A.; Rathore, N.; Schwartz, D. C.; de Pablo, J. J. *J. Chem. Phys.* **2007**, *126*, 084901.
- (32) Yakovchuk, P.; Protozanova, E.; Frank-Kamenetskii, M. D. *Nucleic Acids Res.* **2006**, *34*, 564.
- (33) Drukker, K.; Schatz, G. C. *J. Phys. Chem. B* **2000**, *104*, 6108.
- (34) Maffeo, C.; Schöpflin, R.; Brutzer, H.; Stehr, R.; Aksimentiev, A.; Wedemann, G.; Seidel, R. *Phys. Rev. Lett.* **2010**, *105*, 158101.
- (35) Marrink, S. J.; Risselada, H. J.; Yefimov, S.; Tieleman, D. P.; de Vries, A. H. *J. Phys. Chem. B* **2007**, *111*, 7812.
- (36) Chu, J. W.; Izvekov, S.; Voth, G. A. *Mol. Simul.* **2006**, *32*, 211.
- (37) Noid, W. G.; Chu, J. W.; Ayton, G. S.; Krishna, V.; Izvekov, S.; Voth, G. A.; Das, A.; Andersen, H. C. *J. Chem. Phys.* **2008**, *128*, 244114.
- (38) Noid, W. G.; Liu, P.; Wang, Y.; Chu, J. W.; Ayton, G. S.; Izvekov, S.; Andersen, H. C.; Voth, G. A. *J. Chem. Phys.* **2008**, *128*, 244115.
- (39) Voth, G. A. *J. Chem. Theory Comput.* **2006**, *2*, 463.
- (40) Kale, L.; Skeel, R.; Bhandarkar, M.; Brunner, R.; Gursoy, A.; Krawetz, N.; Phillips, J.; Shinozaki, A.; Varadarajan, K.; Schulten, K. *J. Comput. Phys.* **1999**, *151*, 283.
- (41) Berendsen, H. J. C.; Vanderspoel, D.; Vandrunen, R. *Comput. Phys. Commun.* **1995**, *91*, 43.
- (42) MacKerell, A. D.; Bashford, D.; Bellott, M.; Dunbrack, R. L.; Evanseck, J. D.; Field, M. J.; Fischer, S.; Gao, J.; Guo, H.; Ha, S.; Joseph-McCarthy, D.; Kuchnir, L.; Kuczera, K.; Lau, F. T. K.; Mattos, C.; Michnick, S.; Ngo, T.; Nguyen, D. T.; Prodhom, B.; Reiher, W. E.; Roux, B.; Schlenkrich, M.; Smith, J. C.; Stote, R.; Straub, J.; Watanabe, M.; Wiorkiewicz-Kuczera, J.; Yin, D.; Karplus, M. *J. Phys. Chem. B* **1998**, *102*, 3586.
- (43) Haile, J. M. *Molecular Dynamics Simulation: Elementary Methods*, Wiley-Interscience; 1992.
- (44) Luan, B.; Aksimentiev, A. *Phys. Rev. E: Stat., Nonlinear, Soft Matter Phys.* **2008**, *78*, 021912.
- (45) Humphrey, W.; Dalke, A.; Schulten, K. *J. Mol. Graphics* **1996**, *14*, 33.
- (46) Catlett, C.; Allcock, W. E.; Andrews, P.; Aydt, R.; Bair, R.; Balac, N.; Banister, B.; Barker, T.; Bartelt, M.; Beckman, P.; et al. *High Performance Computing and Grids in Action*; Grandinetti, L., Ed.; Advances in Parallel Computing 16; IOS Press: Amsterdam, 2008.